DNA Curvature in Solution Measured by Fluorescence Resonance Energy Transfer

Katalin Tóth,* Volker Sauermann,‡ and Jörg Langowski

Division Biophysics of Macromolecules, German Cancer Research Center, Im Neuenheimer Feld 280, D-69120 Heidelberg, Germany

Received December 22, 1997; Revised Manuscript Received March 13, 1998

ABSTRACT: The sequence-induced curvature of DNA fragments free in solution was characterized by measurements of the end-to-end distance using fluorescence resonance energy transfer (FRET). The 31 bp oligonucleotides were labeled at their 5′ ends with fluorescein as the donor and rhodamine X as the acceptor. We compared a curved oligonucleotide with three phased A_6 blocks and a control containing $(AT)_3$ instead of the A_6 blocks. The increased efficiency of energy transfer of the A_6-containing DNA indicates the existence of a permanent sequence-induced curvature, the magnitude of which is in good agreement with estimates from theoretical curvature predictions. Energy transfer efficiency and correspondingly curvature increases with NaCl concentration.

The three-dimensional folding of DNA in the cell is important both from a purely mechanical point of view (i.e., how can two meters of DNA fiber be packaged into a nucleus less than 10 μm in diameter), as well as for its biological function, e.g., in long-range transcriptional regulation when an enhancer interacts with a promoter several thousand base pairs away (*1*). DNA is a rather stiff polymer, with a persistence length of 50 nm, but it exists in most circumstances in a compact state: for instance, in chromatin, where the curvature radius of DNA around the nucleosome is about 5 nm, or in virus particles. DNA must be strongly bent in all these cases, and it has been suggested that local structure variations such as sequence- or protein-induced curvature can support the required distortion of the DNA.

The first correlation between DNA sequence, local structure variations, and DNA bending was pointed out by Trifonov and Sussman (*2*), who observed in a Fourier analysis of nucleosome-containing DNA sequences a repetition of AA dinucleotides with a period of 10.5 base pairs/turn, corresponding to the helix pitch of B-DNA. Their hypothesis was that certain sequence elements in DNA could induce a permanent curvature of the helix axis when repeated in phase with the helix pitch. This was later confirmed in numerous cases by the discovery that natural and synthetic DNA sequences with repeating A-blocks showed anomalously slow migration (gel migration anomaly, GMA) on polyacrylamide gels (as reviewed in (ref *3*), and could be ligated into small circles with much higher efficiency than random sequences (for a review see ref *4*). Permanent curvature has also been observed for some DNAs in electron microscopy (*5*−*7*). The standing interpretation of all these results is that blocks of at least four adjacent adenines cause local deviations in the helix axis that will accumulate to an overall curve when repeated in phase with the helix pitch. Such repeated A_n ($n > 3$) blocks were identified in kinetoplast DNA (*8*) and at the origin of replication of λ phage (*9*), where both GMA and increased cyclization probability were found, and in a human mitochondrial DNA sequence by GMA (*10*). In all those cases the biological function requires curvature of the DNA.

The common characteristic of the methods for curvature detection mentioned so far is that the conformation of the DNA is not determined in its free solution state: the mobility of the chain in the gel, on the electron microscope grid or bound to a ligase, is restrained. Only very few free solution measurements of curved DNA structure have been published: Electric dichroism measurements on 267 bp DNA restriction fragments from the kinetoplast of *Leishmania tarentolae* (*11*) at rather low ionic strength (1.6 mM NaCl) showed a 20% difference in rotational relaxation times between two fragments that were identical in sequence except for circular permutation, which places a curve either in the center or near the end of the molecule. Later an electric dichroism study (*12*) could not confirm a strong curvature on 161−399 bp DNA fragments from *Chironomous thummi*, either at low or at physiological salt concentrations, although they showed a high gel migration anomaly. These results suggested an increased rigidity combined with only a slight curvature. An increased rigidity was also supposed by Levene et al. (*11*); on the other hand, Koo et al. (*13*) assumed the standard value for the persistence length for A-tract sequences. Thus, the issue of A-tract flexibility is still under discussion.

Hydrodynamic parameters of 320 bp DNA fragments were measured by analytical ultracentrifugation and dynamic light scattering, but no difference were found between fragments that show a high degree of GMA and those that do not (*14*), although from curvature modeling a large structural difference had been expected.

One problem with solution structure measurements of DNA fragments longer than the persistence length (150 bp) is that eventual structural changes can be "washed out" by their flexibility. It would be therefore desirable to obtain reliable solution measurements of DNA curvature for shorter fragments. One such study has been done by Sun et al. (*15*), who used NMR on short fragments of 10−12 bp to detect the structural deformation in the presence of a single A tract.

* Corresponding author.
‡ Present address: SAP AG, Neurottstrasse 1, D-69190 Walldorf, Germany.

S0006-2960(97)03135-8 CCC: $15.00
Published on Web 05/19/1998

A study of phased A tracts, however, would be intractable with present NMR technology because it would require the analysis of DNAs at least 20 bp long.

A method that has often been applied for distance measurements in biological macromolecules is fluorescence resonance energy transfer (FRET) (*16*). In this method a donor fluorophore D is used whose emission spectrum overlaps with the excitation spectrum of a nearby acceptor fluorophore A. When the donor is excited, energy can be transferred from D to A by dipole−dipole interaction, causing A to be excited in turn and emit fluorescence. The energy transfer efficiency E and therefore the increase in acceptor fluorescence depends among other factors on the distance R between D and A; it decreases strongly with distance because of the dipole−dipole interaction. E can be calculated from an analysis of the emission spectrum of the sample and related to the distance R between the dyes:

$$E = \frac{1}{1 + (R/R_0)^6} \quad (1)$$

The constant R_0 is called the Förster radius. Its value depends on the dyes and their chemical environment. With conventional organic dyes R_0 values of up to 60 Å can be reached, enabling energy transfer to be measured up to a distance of 120−130 Å.

Because of its strong distance dependence, FRET has also been called a molecular ruler. In the field of nucleic acid structure FRET has been used to analyze the helical arrangement of short DNA fragments (*18*), the geometry of the four-way junction (*19*) or bulge loops (*20*), and the structure of ribozymes (*21*).

The aim of the work in this paper is to measure the distance between the ends of a DNA fragment free in solution by FRET. Since in curved DNA the average dye-to-dye distance is smaller than in a straight DNA fragment with the same number of base pairs, one can use FRET to estimate its curvature. Since the expected bending angle/A tract is of the order of 25°, several phased A tracts will be necessary to affect the end-to-end distance of the fragment sufficiently so that a change in the energy transfer efficiency can be observed. Assuming a Förster distance $R_0 = 60$ Å, which is among the largest known, we can still expect a measurable energy transfer for distances around 100 Å. We therefore chose a fragment length of 31 bp for our measurements, long enough to accommodate three A_6 tracts with a predicted change in end-to-end-distance of 8% according to the Bolshoy algorithm (*22*).

MATERIALS AND METHODS

DNA Fragments. Single-stranded oligonucleotides were purchased from MWG Biotech in Ebersberg (Germany). One strand was labeled with covalently linked rhodamine X (RX; C_6 carbon linker) on the 5′ end, and the complementary sequence was labeled with fluorescein (FL; C_3 carbon linker) on its 5′ end. Nonlabeled DNAs of the same sequence were purchased as well.

The sequences were constructed to fit two requirements: short enough (<120 Å) to be measurable by FRET but having as many as possible phased repetitions of long A tracts to maximize the curvature. The best compromise was found between 3 and 4 helix turns. We chose a length of 31 bp, close to 3 complete helix turns, with repetition periods of 10 and 11 bp.

The sequences used were

'linear' (L):

FL- 5'-CTATATACGG CGTATATACGG CTATATACGG-3

3'-GATATATGCC-GCATATATGCC GATATATGCC-5'-RX

'curved' (C):

FL- 5'-CAAAAAACGG CGAAAAAACGG CAAAAAACGG-3'

3'-GTTTTTTGCC-GCTTTTTTGCC GTTTTTTGCC-5'-RX

As a control, a shorter linear sequence L(29) was also constructed, which was identical to L except for a missing AT-TA in the center.

The curvature of sample C was predicted by our program Curvature (*23*) based on the algorithm by Bolshoy et al. (*22*). We obtained a theoretical value of 80°; sequence L had no curvature.

The donor/acceptor pair fluorescein/rhodamine X was selected because of its high Förster radius [$R_0 = 59.6$ Å (*24*)]. Fluorescein was present as a single isomer (*5*) and was attached to the 5′ end of the DNA via a C_3 amino linker; rhodamine X was a mixture of the 5 and 6 isomers (Molecular Probes) and was attached to the 5′ end of the DNA via a C_6 amino linker. The only difference between the linear and curved sequences is the alternation of A and T bases; the sequence in the immediate environment of the dyes was the same for both samples.

The single-stranded oligonucleotides were HPLC-purified until they showed only one band on a polyacrylamide gel, either by ethidium staining or by direct fluorescence of the label. Since the unlabeled DNA differs significantly in mobility from the labeled one, we supposed that less than 1% of the delivered single strands was unlabeled.

Sample Preparation. For sample annealing we mixed complementary strands at equimolar concentrations in 10 mM Tris-HCl, 0.1 mM EDTA, and 100 mM NaCl at pH = 7.5, incubated at 50 °C for 40 min, and cooled them down slowly to 20 °C. Completeness of annealing was checked with gel electrophoresis (0.5 μg of DNA, 14% polyacrylamide gel, buffer TBE 10%, 150 V, 3 h, ethidium staining and observation with UV light). Less then 1% single strands remained after the reaction. We produced four species of double-stranded DNA fragments: nonlabeled (nl), single-labeled with fluorescein (sF) or with rhodamine X (sR), and double-labeled (dl).

FRET measurements on the *acceptor side* were done on double-labeled samples, diluting them into 2 mL of the annealing buffer without NaCl. NaCl concentration was adjusted stepwise with 10 mM Tris-HCl, 5 M NaCl, and 0.1 mM EDTA, pH = 7.5. Single-labeled samples were used to determine concentration-independent spectral ratios.

For the measurement on the donor side we prepared two samples. In mix 1, half the DNA was double-labeled and the other half was nonlabeled; in mix 2, one-fourth was double-labeled and the rest was a mixture of single-labeled and nonlabeled duplexes. Mix 1 was prepared by mixing equimolar concentrations of nonlabeled and double-labeled samples that had been separately denatured at 80 °C and slowly reannealed; mix 2 was prepared by first mixing the nonlabeled and double-labeled samples and then denaturing

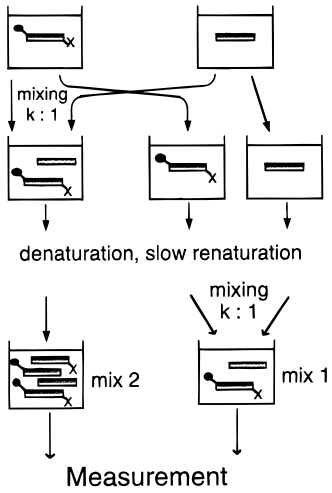

FIGURE 1: Sample mixing scheme for FRET measurements by decreased donor emission: (●) fluorescein label; (×) rhodamine X label.

and reannealing. This way we could ensure that both samples had undergone the same denaturing and reannealing steps. Since the total DNA concentration of the two samples was the same, we could avoid absolute concentration measurements. The mixing procedure is shown in Figure 1.

Low sample concentrations were used to avoid inner filter effects in the fluorescence measurements. Absorbances at the dye absorption maxima were held below 0.03, representing dye concentrations below 500 nM.

Absorption and Emission Spectra. Absorption spectra were measured on a Cary-4E spectrometer (Varian, Mulgrave, Australia) between 220 and 750 nm, with an OD accuracy of 0.001. Emission spectra were measured with an SLM-Aminco 8100 fluorescence spectrometer (SLM, Urbana, IL) using a 150 W xenon lamp. Fluorescence spectra were measured relative to the lamp intensity and corrected for the instrument response and buffer signal. Emission spectra were collected with 4 nm monochromator slit width for excitation and emission light. Excitation wavelengths were 495 nm for the donor and 585 nm for the acceptor. The excitation spectra were detected between 500 and 700 nm. For all measurements the samples were thermostated at 20 °C. Quartz cuvettes with a path length of 1 cm were used. The numerical treatment of the collected data was done with the program KaleidaGraph on a Macintosh computer. For the determination of the energy transfer efficiency, either whole spectra or integrated spectral regions were used: the integration extended over ±5 nm in the absorption spectra and ±10 nm in the emission spectra.

Circular Dichroism. For concentration determination of dye-labeled oligonucleotide duplexes, CD spectra were measured on a Jasco J-710 CD spectrometer in 1 mm rectangular cells (Hellma, Müllheim, Germany). No CD signal was found in the visible region, and the shape of the CD spectrum was the same for dye-labeled and nonlabeled DNA. We then determined the DNA concentration ratio of two samples by dividing their CD spectra and averaging over the regions 235−250 and 260−285 nm.

RESULTS

The efficiency of energy transfer between donor and acceptor was determined both from the enhancement of the acceptor emission and from the decrease of the donor emission in the presence of the acceptor. In our case, when the expected energy transfer efficiency is very small, both types of measurement have several possibilities of error. On the donor side, one compares two samples that should have the same donor concentration, but unfortunately all simple concentration measurements are influenced by the presence of the acceptor in an unknown way. On the acceptor side, the background emission due to overlap with the donor emission and direct excitation of the acceptor is comparable with the enhancement due to the energy transfer and increases the noise, but in a controllable manner.

In the following we describe the procedures that we have followed for determining the energy transfer efficiency on the acceptor and on the donor side.

Energy Transfer Determination from the Enhancement of Acceptor Emission. We measure for a double-labeled sample the following fluorescence spectra: (1) excited at the donor excitation wavelength (495 nm), ${}^{dl}F^{495}$; (2) excited at the acceptor excitation wavelength (585 nm), ${}^{dl}F^{585}$; and (3) the absorption spectrum, ${}^{dl}A$. From independent measurements on single-labeled duplexes we calculate the following concentration-independent spectral ratios: (A) ratio of fluorescein emission at its maximum (520 nm) and at the maximum of the rhodamine X emission (610 nm)

$$ {}^{sF}f = {}^{sF}F^{495}_{520} / {}^{sF}F^{495}_{610} \tag{2} $$

and (B) ratio of the rhodamine X emission at its emission maximum (610 nm) excited at its excitation maximum (585 nm) and at the fluorescein excitation maximum (495 nm)

$$ {}^{sR}f = {}^{sR}F^{585}_{610} / {}^{sR}F^{495}_{610} \tag{3} $$

As the excitation spectrum and the absorption spectrum of rhodamine X are proportional, this last ratio is the same as the ratio of the rhodamine X absorbances at these two wavelengths:

$$ {}^{sR}a = {}^{sR}A_{585} / {}^{sR}A_{495} = {}^{sR}f \tag{4} $$

In our measurements we always used the fluorescence emission ratio instead of the absorbance ratio because it was less noisy.

All spectral ratios are calculated by integrating over a spectral region of ±10 nm for the fluorescence spectra and ±5 nm for the absorption. Using these ratios we can decompose the measured spectrum 1 (${}^{dl}F^{495}$) at the emission maximum of the acceptor into three components:

$$ {}^{dl}F^{495}_{610} = T + D + EE \tag{5} $$

where T is the tail of the emission of the donor

$$ T = {}^{dl}F^{495}_{520} / {}^{sF}f \tag{6} $$

D is the emission due to direct excitation of the acceptor

$$ D = {}^{dl}F^{585}_{610} / {}^{sR}f \tag{7} $$

and EE is the enhanced emission of the acceptor due to energy transfer. Therefore we have

$$EE = {}^{dl}F^{495}_{610} - ({}^{dl}F^{495}_{520}/{}^{sF}f) - ({}^{dl}F^{585}_{610}/{}^{sR}f) \quad (8)$$

Analogously, we can decompose the absorbance of the double-labeled sample ${}^{dl}A$ into the absorbance of its components at the absorption maximum of the donor:

$${}^{dl}A_{495} = {}^{Fdl}A_{495} + {}^{Rdl}A_{495} \quad (9)$$

where the rhodamine X part is calculated as

$${}^{Rdl}A_{495} = {}^{dl}A_{585}/{}^{sR}a \quad (10)$$

and the fluorescein part follows as

$${}^{Fdl}A_{495} = {}^{dl}A_{495} - ({}^{dl}A_{585}/{}^{sR}a) \quad (11)$$

Finally, the efficiency of energy transfer is calculated from the enhanced emission of the acceptor relative to its direct emission, divided by the absorbances of the respective components (*25*):

$$E_A = \frac{EE/{}^{Fdl}A_{495}}{D/{}^{Rdl}A_{495}} \quad (12)$$

Figure 2 summarizes the measured and calculated spectra that were used for calculating the energy transfer efficiency from acceptor enhancement.

The accuracy of this method depends mostly on the quality of the spectra of the double-labeled sample. The fluorescence spectra had a signal-to-noise ratio in the critical region (600−620 nm) greater than 200, and the absorption spectrum at both dye maxima had a signal-to-noise ratio higher than 20.

The factors used in the calculation were obtained by averaging repeated measurements on different single-labeled samples. For rhodamine X, the value of ${}^{sR}f = {}^{sR}a = 16.5 \pm 0.1$ was found for all samples at all ionic strengths. For fluorescein, ${}^{sF}f$ was slightly dependent on the salt concentration; its value was around 21 and was independently determined for every sample preparation. We can conclude that even though a large number of spectral data have to be taken into account for the computation, the relative accuracy calculated from the measurement errors for E_A is ±10%, better than its absolute repeatability of ±0.01.

Energy Transfer Determination from the Decrease of Donor Emission. As outlined in the Materials and Methods section, we prepared two samples at exactly the same DNA, donor, and acceptor concentrations: mix 1 is a 1:1 mixture of double-labeled and unlabeled double-stranded DNA, and mix 2, prepared from mix 1 by denaturation and renaturation, contains double-labeled, single-labeled at acceptor or donor, and unlabeled DNAs at equal concentration. Sample 2 has therefore only half the amount of double-labeled molecules as sample 1.

We measured the fluorescence spectra of samples mix 1, ${}^1F^{495}$, and mix 2, ${}^2F^{495}$, with excitation at the donor wavelength (495 nm). The energy transfer leads to a fluorescence decrease

$$F_{da} = F_d(1 - E_d) \quad (13)$$

where F_{da} is the fluorescence at the donor emission in the presence of the acceptor and F_d is that in its absence. In our mixing scheme, F_d is the same for both samples, and it does not need to be measured independently. In mix 2 only half the donor molecules take part in the energy transfer, so we have

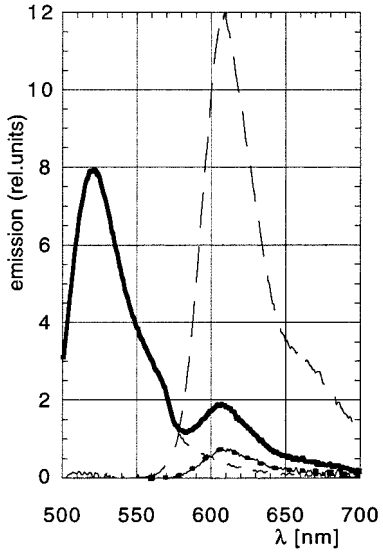

FIGURE 2: Calculation of enhanced acceptor emission: (—) measured spectrum 1, excitation at 495 nm (${}^{dl}F^{495}$) (− − −) measured spectrum 2, excitation at 585 nm (${}^{dl}F^{585}$); (···) calculated direct excitation of the acceptor (*D*); (- - -) calculated normalized fluorescein emission tail (*T*); and (—) calculated enhanced emission (*EE*). Spectra 1 and 2 were taken on the curved sequence at 20 °C in 10 mM Tris-HCl and 500 mM NaCl at pH = 7.5. The calculations are described in the Results section.

$$\frac{{}^1F^{495}_{520}}{{}^2F^{495}_{520}} = \frac{1 - E_d}{1 - E_d/2} \quad (14)$$

This way we avoid absorption measurements for the determination of concentrations of single- and double-labeled samples, such measurements being rather difficult because of the overlap between DNA and dye absorbances, and the very small absorbances involved. However, two minor corrections should be taken into account, which influence E_d only to the second order.

Mixing Ratio k. When the double-labeled and nonlabeled samples are mixed, the mixing ratio may differ from 1:1. Its real value (*k*:1) was determined from CD measurements of the two samples before mixing (see Materials and Methods).

Absolute Concentration Ratio c of Samples 1 and 2. Evaporation or adsorption to the reaction vial could lead to some loss of material during reannealing; this has to be taken into account in the calculation. The value of c can be obtained from measurements of the fluorescence spectra excited at 585 nm, where only rhodamine X will be excited.

$$c = \frac{{}^1F^{585}_{610}}{{}^2F^{585}_{610}} \quad (15)$$

The corrected equation for E_d is

$$E_d = \frac{1 - x}{1 - x/(1 + k)} \quad \text{where} \quad x = \frac{{}^1F^{495}_{520}}{{}^1F^{585}_{610}} \frac{{}^2F^{585}_{610}}{{}^2F^{495}_{520}} \quad (16)$$

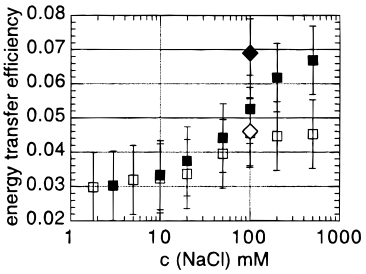

FIGURE 3: Dependence of the energy transfer efficiency, on the NaCl concentration determined from enhanced acceptor emission on the curved (■) and the linear (□) sequence and from decreased donor emission on the curved (◆) and the linear (◇) sequence.

Accuracy. For this method fewer spectra have to be taken, and they can be determined with better signal-to-noise ratio (>300). The k value can be determined with ±5% relative error, but its effect is small: around $E = 0.1$, a 100% variation in k causes only a 10% variation in E. The repeatability of E_d was found to be ±0.01.

For estimating whether the expected small change in energy transfer could be measured by our method, we compared two linear DNAs of 31 and 29 base pairs. [samples L and L(29)]. Here the energy transfer values measured from the decrease of the donor emission at 100 mM NaCl were 4.6% ± 1% for the 31 bp and 10.7% ± 1.5% for the 29 bp long linear fragment, well distinguishable. The corresponding distance difference of 14% ± 7% was in reasonable agreement with the predicted change in end-to-end distance of approximately 7%.

FRET Measurements Show the Presence of Curvature of Short DNA in Solution. Energy transfer efficiencies were determined from the enhancement of acceptor emission at different salt concentrations and from the decrease of donor emission at 100 mM NaCl. All data are presented in Figure 3, which shows that above 10 mM NaCl the efficiency of energy transfer of the curved DNA tends to be higher than that of the linear one. While the measurements on the donor and the acceptor side agree very well for the linear DNA, the curved samples show some difference between the two methods. This deviation may be rationalized by variations between sample preparations or the generally larger error for the donor-side measurement.

Energy Transfer and Curvature Angle Increase with NaCl Concentration. Figure 3 shows a significant increase of the efficiency of energy transfer above 10 mM salt concentration for both sequences. The increase is more pronounced for the curved sequence; the difference between the energy transfer efficiencies of the two sequences increases with salt concentration. The salt-dependent change of the efficiency of energy transfer may be due to changes in the dye-to-dye distance and/or changes in the fluorescence characteristics of the dyes, which influence the Förster radius R_0.

To separate these two effects, we studied the spectroscopic characteristics of single-labeled double-stranded DNAs. Rhodamine X seems to be very stable: neither absorbance nor fluorescence changes between 3 and 500 mM NaCl. On the contrary, the fluorescein absorbance shows a 50% increase from 3 to 500 mM NaCl, while the emission varies nonmonotonically. These changes influence the value of the Förster radius:

$$R_0 = 0.211(n^{-4}Q_d\kappa^2 J)^{1/6} \qquad (17)$$

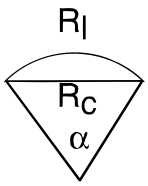

FIGURE 4: Calculation of the curvature angle (α) from the contour length (corresponding to R_l) and the end-to-end distance (R_c) of the curved sequence.

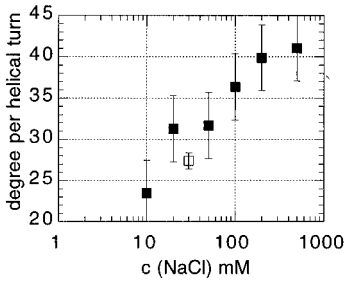

FIGURE 5: Specific curvature angle as a function of NaCl concentration calculated from the FRET measurements (■) and computer prediction corresponding to 30 mM NaCl (□).

where Q_d is the quantum yield of the donor in the absence of the acceptor, J is the overlap integral, κ is the orientation factor, and n is the refractive index of the medium. As the dyes in both samples have the same nucleotide neighbors, one may suppose that their orientation factors behave in the same manner as a function of salt.

From the measured absorbances and emissions we calculated the relative changes in the quantum yield and the overlap integral for both sequences as a function of NaCl concentration and took into account preparation-dependent quantum yield variations as well. We obtained the salt-dependent ratios of the Förster radii R_{c0}/R_{l0} and could then calculate the relative dye-to-dye distances for the two DNAs, R_c/R_l:

$$\frac{R_c}{R_l} = \frac{R_{c0}}{R_{l0}}\left[\frac{E_l(E_c - 1)}{E_c(E_l - 1)}\right]^{1/6} \qquad (18)$$

Supposing that the linear sequence remains straight under the salt conditions used, R_c/R_l represents the ratio of the end-to-end distance of the curved molecule to its contour length and is presumably independent of the optical properties of the dyes. Approximating the geometry by a circular arc as shown in Figure 4, one can calculate the curvature angle α (expressed in radians) from

$$\frac{\sin(\alpha/2)}{\alpha/2} = \frac{R_c}{R_l} \qquad (19)$$

We define the specific curvature α_s as the curvature angle in degrees per helical turn. Figure 5 presents the specific curvature of our A_6 sequences as a function of salt concentration. A strong increase is observed between 10 and 500 mM NaCl: the specific curvature angle changes from 23° ±4° to 41° ± 4°.

Dye-to-Dye Distance Decreases at Higher Salts. Up to now we calculated energy transfer efficiencies and relative dye-to-dye distances directly from the measured fluorescence and absorption spectra. For determining absolute dye-to-dye distances we need two more parameters: the Förster radius

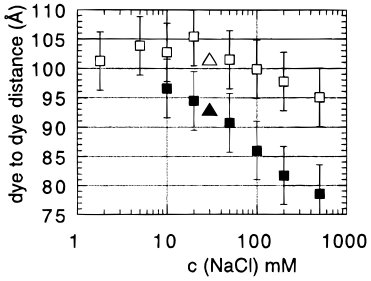

FIGURE 6: Dye-to-dye distance as a function of NaCl concentration as determined from the FRET measurements for curved (■) and linear (□) sequences and calculated end-to-end distance from curvature prediction for curved (▲) and linear (△) sequences.

(R_0) and the orientation factor (κ). Lacking a better alternative, these parameters were adopted from literature data where the dyes were bound to DNAs in the same way as in our case (*24*). The values taken are $R_0 = 59.6$ Å for the linear sequence at 0.1 M NaCl, and $\kappa^2 = {}^2/_3$ in all cases. The use of the value ${}^2/_3$ for κ^2 can be justified by anisotropy measurements: the measured anisotropy of rhodamine X is 0.2 ± 0.02 at all ionic strengths in both samples, and the values for fluorescein were between 0.05 and 0.07. It has been shown (*26*) that using $\kappa^2 = {}^2/_3$ with anisotropies of this size leads to an error in the determination of the mean dye-to-dye distance of less than 1%, which is generally accepted in FRET applications (*18*, *24*).

The calculated dye-to-dye distances are presented in Figure 6. The curved sequence shows a significant monotonic decrease in the dye-to-dye distance of about 20% between 10 and 500 mM NaCl. The dye-to-dye distance of the linear sequence is significantly higher in this salt concentration range than that of the curved sequence. The slight salt-dependent decrease of the dye-to-dye distance of the linear sequence might reflect either a real decrease of the DNA end-to-end distance or a salt dependence in the Förster radius or the mobility of the dyes (we also note that the energy transfer efficiency for the linear DNA stays constant above 100 mM salt while the apparent end-to-end distance still decreases).

At 100 mM salt the good agreement of the apparent dye-to-dye distance for the linear fragment with the end-to-end distance of a 31 bp DNA supports our choice for the values of R_0 and κ. We also assume that these values are the same for the curved sequence since the base pairs immediately adjacent to the dyes are the same for the two fragments. While the absolute values for the end-to-end distance might be influenced by a salt dependence of the dye orientation and/or the Förster radius, the curvature values are calculated from the distance ratios R_c/R_l and eventual changes in the ratio of the Förster radii R_{c0}/R_{l0}. Thus, they will be independent of salt-dependent effects in first approximation. For a better understanding of the photophysics of fluorescent labels attached to DNA, this problem may merit further investigation, but this is beyond the scope of our present report.

Comparison with Model Predictions. The Bolshoy model (*22*; *23*) predicts an end-to-end distance of $L_l = 101.6$ Å and $L_c = 93$ Å for the linear and curved sequences, respectively. The parameters in this model are mostly related to gel experiments in buffers of 40 mM monovalent ions (Tris-HCl); thus they have to be compared to the experimental data at 30 mM NaCl, which also contained 10 mM Tris-HCl.

Table 1: Energy Transfer Efficiencies and Averaged Dye-to-Dye Distances at 30 mM Na^+ [a]

	E_L (%)	E_C (%)	R_L (Å)	R_C (Å)	R_l/R_C
dyes isotropically mobile (1)	5.2	8.6	96.6	88.4	1.09
dyes fixed at DNA ends (2)	3.9	6.5	101.6	93	1.09
dyes mobile, excluded (3)	3.6	5.8	103	94.8	1.09
experiment	3.6 ± 1	4 ± 1	103 ± 5	93 ± 5	1.10 ± 0.1

[a] Calculated from eq 20 for different assumptions about the dye geometry (see text) and compared to values interpolated from experimental data.

To estimate the theoretical dye-to-dye distance, we also have to take into account the lengths of the linker arms of the dyes, and we have to average the efficiency of energy transfer over all possible different orientations of the dyes with respect to the DNA. The lengths of the two linker arms were taken as 7.5 Å (C_3 linker) and 13.5 Å (C_6 linker). For the averaging we used a simplified distribution of the dye-to-dye distance with uniform probability between their maximal and minimal extended positions. The averaged energy transfer efficiency was calculated by assuming a Förster radius of 59.6 Å and integrating eq 1:

$$\bar{E} = \frac{\int_{R_{min}}^{R_{max}} \frac{dR}{1 + (R/R_0)^6}}{R_{max} - R_{min}} \qquad (20)$$

Different geometrical approaches were used to estimate the theoretical average energy transfer efficiency. An upper estimate (1) is that the dyes are isotropically mobile, i.e., the linker arms may bend back into the DNA without steric hindrance.The simplest estimate (2) is to set the average dye-to-dye distance equal to the DNA end-to-end distance. A more realistic geometry (3) is to suppose that the dyes may bend back to the DNA but cannot touch it. Table 1 presents the calculated mean energy transfer efficiencies and the averaged dye-to-dye distances for these three cases, as well as values interpolated from the measurements for 30 mM salt.

These results show that the theoretical energy transfer efficiencies are quite sensitive to the chosen geometry. Our experimental results are inside the range covered by the different approaches. This fact strengthens our assumptions concerning R_0 and κ^2, but the data do not allow us to favor a choice between the geometries. On the other hand, the relative lengths of the two sequences ($R_l/R_c = 1.09$) and therefore the specific curvature angle do not depend on the dye-arm geometry, which justifies the use of these simplified models. The averaged value of 27.3° as calculated from the curvature predictions for an assumed ionic strength of 30 mM excess NaCl agrees within error limits with the value of 28.7° ± 4° interpolated from our measurements (see Figure 5).

DISCUSSION

The most important results of this work are a direct demonstration of sequence-induced DNA curvature in free

solution and the characterization of NaCl-dependent changes of the curvature.

The demonstration of curvature in solution was possible by choosing a short DNA sequence with very high predicted curvature and the high sensitivity of FRET for distance measurements in biopolymers. Earlier studies in solution were done with methods that require either very low ionic strength (electric dichroism) or longer DNA (light scattering, ultracentrifugation), circumstances that may diminish the effect of curvature.

The sensitivity and accuracy of the FRET measured by steady-state emission could be increased by a sample preparation technique that avoids direct concentration measurements. FRET measurements are routinely used in the region of 10−60% energy transfer efficiency, but even in that well-measurable region, comparison between donor- and acceptor-side measurements is often missing or shows inconsistency in the literature. With simple emission measurements on the set of donor-only or acceptor-only labeled and double-labeled samples we confronted the same difficulty. Therefore we applied two different sample preparation and data analysis methods to obtain consistent energy transfer efficiencies from measurements on the donor and acceptor sides at the 3% to 10% level. At this low transfer efficiency the data analysis also had to be refined: in the detection of the enhanced acceptor emission the background contributed by the emission tail of the donor and direct excitation of the acceptor is as high as the contribution from energy transfer. We used spectral integration instead of single-wavelength measurements and concentration-independent spectral ratios, which increased the reproducibility.

The FRET-detected specific curvature is strongly salt-dependent, increasing from 23° to 41° per A_6 block between 10 and 500 mM NaCl. This result is in some contradiction with other studies: in gel electrophoresis below 60 mM NaCl (*27*) or in electric dichroism measurements below 10 mM NaCl concentration (*11*), no change or even a decrease of the curvature caused by monovalent salts was reported. Other methods such as cyclization kinetics or crystallization are very limited in their choice of salt concentrations; neither have electron microscopic studies of DNA curvature focused on monovalent salt dependence. The theoretical models used in the field also do not incorporate ionic effects. The discrepancy between our FRET observations and the gel migration experiments suggests that Na^+ concentrations > 10 mM have a different influence on the geometry of DNA in solution than on the gel anomaly.

Using the Bolshoy model whose parameters correspond to 40 mM monovalent ions, we obtain a curvature angle of 27.3°/A tract for the same sequence, in good agreement with our measurements. Recent fluorescence polarization anisotropy measurements on the same, nonlabeled sequences also prove the presence of curvature with a comparable angle (Toth et al., unpublished data). A quantitative comparison to results obtained on other sequences containing phased A_6 tracts is difficult because of the salt dependence discussed above. Koo et al. (*13*) fitted results from ring-closure experiments in the presence of 70 mM Tris and 10 mM $MgCl_2$ with Monte Carlo simulations and obtained a curvature angle of 17−21°/A_6 tract. Taking into account that Mg^{2+} ions are supposed to increase the curvature (*27*−*29*), this value is somewhat lower than in our case. However, the effects of Mg^{2+} as well as other ions and temperature effects have not yet been studied on molecules free in solution. FRET seems to be a good method of choice to continue such investigations.

ACKNOWLEDGMENT

We thank Nathalie Brun for expert technical assistance and Karsten Rippe for critical reading of the manuscript.

REFERENCES

1. Rippe, K., von Hippel, P. H., and Langowski, J. (1995) *Trends Biochem. Sci. 20*, 500−506.
2. Trifonov, E. N., and Sussman, J. L. (1980) *Proc. Natl. Acad. Sci. U.S.A. 77*, 3816−3820.
3. Diekmann, S. (1992) *Methods Enzymol. 212*, 30−46.
4. Crothers, D. M., Drak, J., Kahn, J. D., and Levene, S. D. (1992) *Methods Enzymol 212*, 3−29.
5. Barcelo, F., Pons, J., Petitpierre, E., Barjau, I., and Portugal, J. (1997) *Eur. J. Biochem. 244*, 318−324.
6. Dubochet, J., Bednar, J., Furrer, P., Stasiak, A. Z., Stasiak, A., and Bolshoy, A. A. (1994) *Nat. Struct. Biol. 1*, 361−363.
7. Muzard, G., Théveny, B., and Révet, B. (1990) *EMBO J. 9*, 1289−1298.
8. Marini, J. C., Levene, S. D., and Crothers, D. M. (1982) *Proc. Natl. Acad. Sci. U.S.A. 79*, 7664−7668.
9. Zahn, K., and Blattner, F. R. (1985) *Nature 317*, 451−453.
10. Welter, C., Dooley, S., Zang, K. D., and Blin, N. (1989) *Nucleic Acids Res. 17*, 6077−6086.
11. Levene, S. D., Wu, H. M., and Crothers, D. M. (1986) *Biochemistry 25*, 3988−3995.
12. Pörschke, D., Schmidt, E. R., Hankeln, T., Nolte, G., and Antosiewicz, J. (1993) *Biophys. Chem. 47*, 179−191.
13. Koo, H. S., Drak, J., Rice, J. A., and Crothers, D. M. (1990) *Biochemistry 29*, 4227−4234.
14. Kremer, W. (1992) Hydrodynamische Charakterisierung von superhelikaler DNA und DNA-Fragmenten, Doctoral thesis, University of Göttingen, Göttingen, Germany.
15. Sun, D., Lin, C. H., and Hurley, L. H. (1993) *Biochemistry 32*, 4487−4495.
16. Clegg, R. M. (1996). Fluorescence resonance energy transfer, in *Fluorescence imaging spectroscopy and microscopy* (Wang, X. F., and Herman, B., Eds.) pp 179−252, John Wiley and Sons, New York.
17. Förster, T. (1946) *Naturwissenschaften 6*, 166−175.
18. Clegg, R. M., Murchie, A. I. H., Zechel, A., and Lilley, D. M. J. (1993) *Proc. Natl. Acad. Sci. U.S.A. 90*, 2994−2998.
19. Clegg, R. M., Murchie, A. I. H., Zechel, A., Carlberg, C., Diekmann, S., and Lilley, D. M. J. (1992) *Biochemistry 31*, 4846−4856.
20. Gohlke, C., Murchie, A. I. H., Lilley, D. M. J., and Clegg, R. M. (1994) *Proc. Natl. Acad. Sci. U.S.A. 91*, 11660−11664.
21. Tuschl, T., Gohlke, C., Jovin, T. M., Westhof, E., and Eckstein, F. (1994) *Science 266*, 785−789.
22. Bolshoy, A., McNamara, P., Harrington, R. E., and Trifonov, E. N. (1991) *Proc. Natl. Acad. Sci. U.S.A. 88*, 2312−2316.
23. Schätz, T., and Langowski, J. (1997) *J. Biomol. Struct. Dyn. 15*, 265−275.
24. Parkhurst, K. M., and Parkhurst, L. J. (1995) *Biochemistry 34*, 293−300.
25. Cheung, H. C. (1991) Resonance Energy Transfer, in *Topics in Fluorescence Spectroscopy* (Lakowicz, J. R., Ed.) pp 127−176; Plenum Press, New York.
26. Haas, E., Katchalski-Katzir, E., and Steinberg, I. Z. (1978) *Biochemistry 17*, 5064−5070.
27. Diekmann, S. (1987) *Nucleic Acids Res. 15*, 247−265.
28. Laundon, C. H., and Griffith, J. D. (1987) *Biochemistry 26*, 3759−3762.
29. Han, W., Lindsay, S. M., Dlakic, M., and Harrington, R. M. (1997) *Nature 386*, 563.

BI973135Z